Chemical Engineering Journal 281 (2015) 482–490

Contents lists available at ScienceDirect

Chemical Engineering Journal

journal homepage: www.elsevier.com/locate/cej

SnO_2 quantum dots decorated silica nanoparticles for fast removal of cationic dye (methylene blue) from wastewater

Dipa Dutta, Dinbandhu Thakur, Dhirendra Bahadur *

Department of Metallurgical Engineering & Materials Science, Indian Institute of Technology Bombay, Mumbai, India

HIGHLIGHTS

- Noble approach of decorating MSN with SnO_2 QDs.
- This composite is not exploited so far as adsorbent for removing pollutant.
- The effect of adsorbent dosage, contact time, pH, temperature, salt and initial dye concentration are studied in detail.
- Very fast removal of dye from aqueous solution, ~100% of MB gets adsorbed within just 5 min.
- Maximum monolayer adsorption capacity of 73.15 mg/g is obtained.

GRAPHICAL ABSTRACT

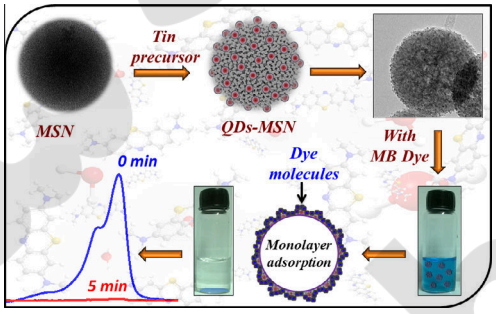

ARTICLE INFO

Article history:
Received 21 April 2015
Received in revised form 24 June 2015
Accepted 25 June 2015
Available online 6 July 2015

Keywords:
Tin dioxide quantum dots
Mesoporous silica nanoparticle (MSN)
Adsorption
Methylene blue

ABSTRACT

Mesoporous SiO_2 nanoparticles (MSN) decorated with SnO_2 quantum dots (QDs) are fabricated via simple two-step method. Morphological investigation shows that the spherical silica particles are uniformly decorated with crystalline SnO_2 quantum dots. The introduction of the SnO_2 quantum dots onto silica particles are also evidenced by the significant change in the specific surface area and zeta potential of the composite. Large BET surface area and uniform pore size distribution with large pore volume suggests that this composite can be exploited as an adsorbent material for organic dyes present in industrial wastewater. At room temperature, it is found to adsorb ~100% of methylene blue (MB), a cationic dye within 5 min. The effects of variables such as the amount of adsorbents, contact time, pH of the initial solution, salt concentration, temperature and initial dye concentration on MB removal are studied in detail. The experimental equilibrium data is investigated using different isotherm models and it is established that Langmuir isotherm model fitted well with maximum monolayer adsorption capacity of 73.15 mg/g. The high adsorption capacity, fast removal rate and reusability of this binary nanocomposite essentially establishes that the material can be used as environment friendly and low cost adsorbent material for cationic dyes.

1. Introduction

Discharge of untreated color effluents from different textile industries to the environment has become a global apprehension due to its harmful impact on flora and fauna [1]. There are more than 100,000 dyes commercially available, and across the globe about 7×10^5 tonnes of dying materials are being used per annum [2]. About 10–15% of used dyes are lost during the dying process and are released to environment as effluents. According to the World Bank (WB), around 17–20% of industrial pollutions originate from color textile waste [3]. In general, aromatic organic dyes are stable in nature and therefore difficult to be biodegraded. Almost all of these dyes are toxic to the ecological system, and also have

* Corresponding author. Tel.: +91 22 2576 7632; fax: +91 22 2572 3480.
E-mail address: dhirenb@iitb.ac.in (D. Bahadur).

http://dx.doi.org/10.1016/j.cej.2015.06.110
1385-8947/

carcinogenic properties. Exposure to methylene blue (MB) may cause permanent injury to the eyes of human and animals [4]. In view of this, it is of immense importance to remove the dyestuff before discharging to water bodies. Various techniques such as membrane filtration, ion exchange, electrochemical, coagulation, chemical oxidation, and adsorption are used for removal of different toxic organic dyes from industrial wastewater. Among all these conventional techniques for removing dyestuff from aqueous medium, adsorption is an effective and attractive technique because of its advantages like small amount of residues, reusability of the adsorbent and simplicity of operation etc. [5,6].

Until very recent times, activated carbon was the most widely used adsorbent for removal of organic dyes, but its use is limited by its high cost, low bio-degradability, presence of macropores and requirement of a large amount of adsorbent for fast removal [3,7,8]. Considerable efforts are being made by many researchers to find appropriate replacement with high adsorption capacity, fast removal and low cost in order to effectively remove dyes from wastewaters. Nanomaterials with high surface to volume ratio is one of the most likely choices for this purpose. Moreover, for macromolecules, the particle diffusion may decrease the adsorption rate and available capacity as well [9]. Hence, it is of significant importance to fabricate a recyclable adsorbent with large surface area and small diffusion resistance for its commercial use. In view of this, much attention has been paid to fabricate different nano adsorbent materials [10]. In recent years, different inorganic oxide materials such as Fe_3O_4 nanoparticles [10], MnO_2 nanosheets [11] and $BiFeO_3$/a-Fe_2O_3 core/shell composite particles [12] have been studied as possible adsorbent for organic dyes. On the other hand, mesoporous silica nanoparticles (MSN) serve as a unique adsorbent material for different organic dyes and also serve as matrix materials for loading of different nanoparticle [3,5,13]. You et al. [14] synthesized silica hematite nanocomposite for removal of MB from aqueous solution. Shamsizadeh and co-workers [15] efficiently removed malachite green-oxalate (MG) dye using tin oxide nanoparticles loaded activated carbon. Semiconducting SnO_2 quantum dots (QDs) are presently attracting consideration due to their noticeable effect in removing pollutants from wastewater [16].

In view of the available literature, SnO_2 QDs loaded MSN may fulfill the requirement of nano adsorbent; which have large surface area and at the same time the presence of SnO_2 QDs decreases the particle diffusion resistance [8]. To the best of our knowledge, SnO_2 QDs decorated MSN (QDs-MSN) is not exploited so far as a possible adsorbent materials for removing pollutants from wastewater. In this work, cationic dye methylene blue (MB) is selected as a model dye to study the performance of QDs-MSN as an adsorbent material for water remediation. Here we present a noble approach of decorating MSN with SnO_2 QDs. The effect of adsorbent dosage, contact time, initial dye concentration, salt concentration, temperature and pH of the initial solution towards adsorption capacity was investigated. Results show that QDs-MSN is an ideal aspirant for removal of positively charged organic dyes from colored wastewater.

2. Experimental methods

2.1. Materials and synthesis

2.1.1. Synthesis of mesoporous silica nanoparticles (MSN)

MSNs was synthesized by modified Stober's method [17] using cetyl trimethyl ammonium bromide (CTAB, 99%, spectrochem) as surfactant material and tetraethyl orthosilicate (TEOS, 98%, Kemphasol) as precursor for SiO_2. In a typical synthesis, 100 mg of CTAB was dissolved in 25 mL water–ethanol mixture (4:1) and an appropriate amount of ammonia solution (NH_4OH, 25%, Merck) was added to the CTAB solution under continuous magnetic stirring. Then 1 mL of TEOS was added drop wise and the temperature of the solution was maintained at 50 °C for 4 h. The obtained product was dried overnight at 60 °C, after washing with ethanol and MilliQ water following centrifugation (6000 rpm for 10 min).

2.1.2. Synthesis of SnO_2 quantum dots (QDs)

$SnCl_4{\cdot}5H_2O$ (98%, Sigma–Aldrich) was used as the precursor. In this method, $SnCl_4{\cdot}5H_2O$ and ammonium hydroxide (10 mL) were added to 40 ml of deionized water, with continuous stirring. NH_4OH instantaneously reacted with $SnCl_4{\cdot}5H_2O$ solution and gave a white precipitation. It was then maintained at room temperature for 8 h with continuous stirring. The obtained product was centrifuged (10,000 rpm for 10 min), washed with ethanol and MilliQ water, and dried overnight at 60 °C in air.

2.1.3. Fabrication of SnO_2 QDs/SiO_2 (QDs-MSN) nanocomposite

In this work, we have synthesized the QDs-MSN nanocomposite by a simple wet chemical method. In a typical synthesis batch, first 50 mg MSN was dissolved in 50 mL water–ammonia solution mixture (4:1) and sonicated for 4 min. Then 245 mg of tin precursor ($SnCl_4{\cdot}5H_2O$) was added to this mixture. The final solution was maintained at room temperature under continuous stirring for 8 h. This was then centrifuged (6000 rpm for 10 min), washed with ethanol and MilliQ water, and dried overnight at 60 °C in air.

2.2. Characterization

Zeta potential of QDs-MSN in water was measured using Zeta analyzer (Delsa Nano C, Beckman Coulter, USA), over a pH range from 3 to 11. X-ray Diffraction (XRD) patterns of the products were obtained using a Philips powder diffractometer PW3040/60 with Cu Kα (1.5406 Å) radiation for probing the crystallite size as well as phase purity. The size, morphology and elemental mapping of the samples were explored using a high-resolution transmission electron microscopy (HRTEM), JEOL JAM 2100F (200 kV). The surface morphologies of the samples were characterized using a field emission scanning electron microscope (FESEM, JEOL, JSM-7600F) on Si (100) substrate. Following thorough de-gassing of the samples at 150 °C for 4 h, porosity and surface area measurements were executed using N2 absorption desorption isotherm, in a surface area and porosity analyzer (Micromeritics ASAP 2020).

2.3. Adsorption measurement

Optimized dose of the adsorbent composite was obtained by measuring removal efficiency of MB, for different doses of the composite with 80 mL of 10 ppm of aqueous MB. In different batches, optimized dose of the composite was dispersed in 80 ml of different concentrations (10–50 ppm) of aqueous MB. These mixtures were continuously stirred for 1 h in dark. During this adsorption experiment, aliquots of 1 mL each was collected at an interval of 1 min for 5 min and then at interval of 5 min for 55 min. The collected aliquots were subsequently centrifuged at 1000 rpm for 5 min. The concentration of MB in supernatant solution was measured using UV–Vis spectroscopy (Cintra 202). To compare constitute materials efficiency towards MB adsorption, three different adsorption experiments were carried out using 80 mL of aqueous MB (10 ppm) with SnO_2 QDs, MSN and the composite. All these adsorption experiments were conducted at a pH of 6.1. The impact of initial pH on adsorption process was investigated by varying the pH of the dye solution using HCl and NaOH before adding the adsorbent material. The effect of salt concentration on the adsorption capacity or capture percentage by QDs-MSN was examined with increasing NaCl or $CaCl_2$ concentrations ranging from 0 to

0.1 M, while other parameters were kept constant. The adsorption stability of the composite was studied by reusing the same composite material in four batches of MB adsorption experiments. In all the four batches, 80 ml of an aqueous MB (10 ppm) solution was mixed with 50 mg of the composite and stirred for 5 min at room temperature. The QDs-MSN used in the first experiment, was subsequently removed from the solution by centrifugation and washed with MilliQ water. The washed composite was then reused in the second batch of absorption experiment and so on.

3. Results and discussions

3.1. Materials characterization

Rate of hydrolysis of TEOS by ammonia, and condensation of Si–OH to form siloxane are the two key factors in controlling the particle size of the silica thus obtained [17–19]. It is therefore essential to understand the influence of the ammonia concentration on the size of the MSN. Three different sets of reactions were carried out using different ammonia concentrations, whereas other experimental conditions remained the same. MSNs' size increases with the increase in ammonia concentration used for the synthesis.

The XRD pattern of silica (Fig. 1(a)) shows a broad peak at $2\theta = 22.7°$, corresponding to the amorphous nature of silica. Fig. 1(b) and (c) represents XRD patterns of SnO_2 QDs and the composites, respectively. The XRD analysis of SnO_2 QDs and QDs-MSN reveals that all the diffraction peaks can be indexed to the tetragonal rutile SnO_2 structure (ICDD file No. -41-1445). All the diffraction peaks of SnO_2 QDs and the composites are broad, indicating smaller crystallite size. No other additional phase was detected. Bare SnO_2 QDs exhibit a single phase rutile structure with an average crystallite size of ~3 nm (averaged from (1 1 0), (1 0 1) and (2 1 1) peaks) and lattice constant $a = b = 4.7382$ (Å) and $c = 3.1871$ (Å). In case of QDs-MSN, two most intense SnO_2 peaks are merged with the hump from amorphous silica, and appeared as an asymmetric peak. Apart from this asymmetric peak, diffraction peaks corresponding to the crystalline planes of tetragonal SnO_2 phase are observed. Hence, XRD indicates the inclusion of SnO_2 QDs within the silica matrix.

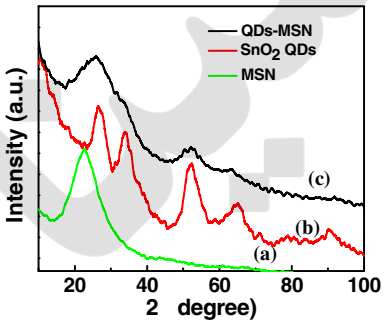

Fig. 1. Shows the XRD patterns of (a) amorphous MSN, (b) crystalline SnO_2 QDs and (c) QDs-MSN.

The morphology of the QDs-MSN and its individual constituent were studied by FEGSEM and HRTEM. FEGSEM and HRTEM images of MSN are shown in Fig. S1(a)–(d) (ESI) respectively. Morphological study shows that the size of the MSN synthesized using 0.3 mL of ammonia solution, is around 150–160 nm. HRTEM image and selected area electron diffraction pattern of SnO_2 QDs are shown in Fig. S2(a) and (b) (ESI) respectively. Fig. S2(a) describes the single crystalline nature of the spherical QDs with a size distribution of 3 ± 0.5 nm. The interplanar spacing estimated from the image (S2(a)) is 0.34 nm. This can be indexed to the (1 1 0) plane of rutile SnO_2, which again shows a good agreement with the XRD results. The SAED patterns obtained from these QDs exhibit a ring pattern. These rings can be indexed to the tetragonal SnO_2 structure and the brightest ring relates to the (1 1 0) plane.

HRTEM images of QDs-MSN shows that ~3 nm SnO_2 quantum dots are homogeneously distributed on the surface of 160 nm mesoporous silica. The interplanar spacing for the composite, estimated from the HRTEM image (Fig. 2(d)), is 0.34 nm. This can be indexed to the (1 1 0) plane of rutile SnO_2, which is again consistent with the HRTEM results of bare SnO_2 QDs. The scanning transmission electron microscopy (STEM) images of the QDs-MSN composite (Fig. 2(e)) and the corresponding elemental mapping confirms uniform decoration of SnO_2 QDs on spherical SiO_2 matrix. White, red and green colors represent the elements O, Si and Sn, respectively.

FEGSEM images of the composite with particle size distribution are shown in Fig. S3 (ESI). A considerable change in the morphology of the composite is observed as compared to its constituent

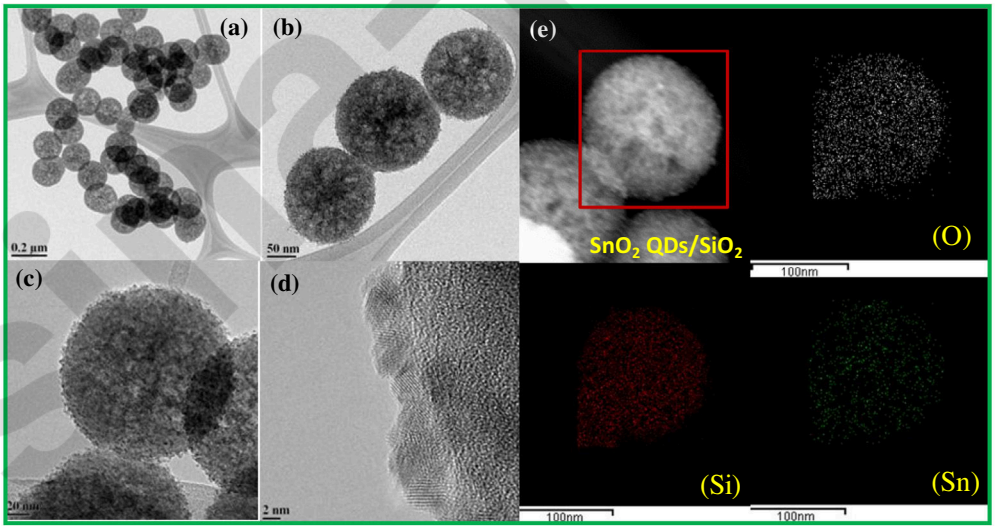

Fig. 2. (a–d) The HRTEM image of QDs-MSN nanocomposite at different magnification. (e) The STEM image of QDs-MSN nanocomposite and corresponding elemental mapping.

bare MSN. From different microscopic images, it is evident that SnO_2 QDs are evenly decorated on the surface of the SiO_2 matrix. Wang et al. [20] also synthesized SnO_2 nanoparticles coated SiO_2 microspheres, but the distribution of SnO_2 QDs was non-uniform. However, this synthesis method took much longer time ~100 h, as compared to our method reported here.

To understand the textural properties, like surface area and pore volume, of the composite and its individual counterparts, Brunauer–Emmett–Teller (BET) surface area and pore volume measurements were studied in detail. Fig. 3(a) shows the N_2 physisorption isotherms of the QDs-MSN. The incorporation of QDs onto SiO_2 matrix does not change the characteristics of the N_2 adsorption–desorption isotherm of SiO_2 matrix. N_2 physisorption isotherms of the MSN and SnO_2 QDs are shown in Fig. S4(a) and (b) (ESI) respectively. The composite exhibits a hysteresis loop for P/P_0 in the range of 0.42–1.0. The hysteresis loop for the composite and MSN resembles the H3 type as per the IUPAC classification. For bare QDs the adsorption branch rises very slowly to higher relative pressure points whereas the desorption branch moves slowly to the middle P/P_0 point (0.41) and decreases suddenly, showing a clear H2 type loop [21]. In such cases, the pore shape is not well-defined [22]. MSN which were synthesized using 0.3 mL ammonia solution, has the highest BET surface area of 524.51 m^2/g followed by the composite (306 m^2/g) and SnO_2 QDs (286 m^2/g).

Comparison of the calculated pore size distribution of the constituents and the QDs-MSN composite clearly suggests the presence of mesopores as per the IUPAC nomenclature. The details of texture analysis and surface charge of MSN, SnO_2 QDs and the composite are listed in Table 1. The surface area of the composite decreases with the incorporation of SnO_2 QDs, which confirms the presence of QDs not only on the surface of the silica but also in the interior of the SiO_2 matrix. The total pore volume (single point adsorption) of the composite is 0.45 cm^3/g, larger than that of SnO_2 QDs.

Generally, the surface area and polarity of the materials are two key factors in adsorption process. As compared to its individual constituents, the composite registered higher values of negative zeta potential. Though the surface area of the composite material is less than that of MSNs, but due to higher negative zeta potential of the composite, it can be used as an efficient adsorbent for cationic dyes like MB.

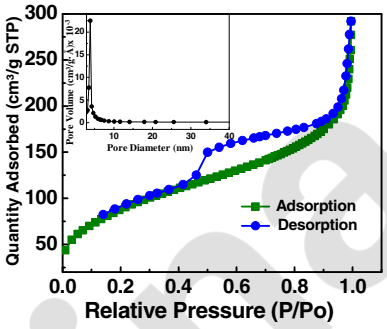

Fig. 3. Nitrogen adsorption–desorption isotherm curves of QDs-MSN. Inset shows the pore size distribution curve of the composite.

Table 1
Comparison of the texture and surface properties of the composite and its constituent materials.

Materials	Size (nm)	Surface area (m^2/g)	Pore volume (cm^3/g)	Zeta potential (mV)
MSN	160	524.51	0.440	−36.35
SnO_2 QDs	3	286.54	0.276	−37.56
QDs-MSN	170	306.29	0.451	−48.05

3.2. Adsorption properties

3.2.1. Effect of adsorbent dosage

The relation between the concentration of the adsorbent and the capture efficiency of adsorbent was studied in detail. Percentage of capture efficiency was calculated using Eq. (1) [23]

$$\%\ \text{Capture} = \frac{C_o - C_e}{C_o} \quad (1)$$

C_o is the initial whereas C_e is the equilibrium concentration of dye in mg/L. Due to increase in the number of active sites, the UV–Vis absorption intensity of dye (at 665 nm) decreases on increasing the concentration of QDs-MSN from 0 to 625 mg/L as shown in Fig. 4. At room temperature, it was found to adsorb ~100% of MB (10 ppm) using 625 mg/L QDs-MSN, within 5 min. For all the isotherms and kinetic studies, adsorbent concentration was fixed at 625 mg/L. The dye capture ability can also be visualized directly by observing the color changes of the dye solutions with and without adding QDs-MSN into it (lower inset of Fig. 4(b)). The excellent rate of adsorption can be attributed to (i) the electrostatic attraction between the negatively charged QDs-MSN and cationic dye MB, (ii) the large specific surface area (306 m^2/g) and the mesoporous structure of QDs-MSN, (iii) and low diffusion resistance of dye onto nanocomposite [10].

3.2.2. Effect of initial MB concentration and adsorption isotherms of MB

Adsorption isotherms furnish information on the relation between adsorption capacity and equilibrium adsorption concentration of the adsorbate in the solution. The mode of interaction of adsorbate molecules with adsorbent is best described by the fitted isotherms. The adsorption capacity is defined as the amount of dye adsorbed per unit weight of adsorbent. The adsorption capacity Q_e was calculated using the mass balance Eq. (2) [3]

$$Q_e = \frac{C_o - C_e}{M} V \quad (2)$$

V is initial volume of the solution (L), and M is the weight of adsorbent (g). The adsorption of dyes for different initial dye concentrations (10–50 ppm) was investigated at room temperature, for an adsorption period of 1 h. All these adsorption isotherm experiments were conducted at a pH of 6.1. The adsorption isotherm of MB for QDs-MSN at different initial dye concentrations is depicted in Fig. S5.

As the Langmuir as well as Freundlich models are widely being used in solid–liquid adsorption systems, both are tested in this work. These two models follow some assumption that might not be physically valid in real systems, but these provide a quantitative estimation of important adsorption parameters. Langmuir isotherms are applicable to the homogeneous surfaces, which have equal adsorption affinity sites, while Freundlich model assumes heterogeneous adsorption sites.

The linear form of Langmuir isotherms can be describes as [24]

$$\frac{C_e}{Q_e} = \frac{1}{K_L Q_{max}} + \frac{C_e}{Q_{max}} \quad (3)$$

where all the parameters are the same as defined before. K_L and Q_{max} are the Langmuir adsorption constant (L/mg) and maximum monolayer adsorption capacity, respectively. A dimensionless parameter R_L is used to express important characteristics of this isotherm, and it is expressed by Eq. (4) [2]

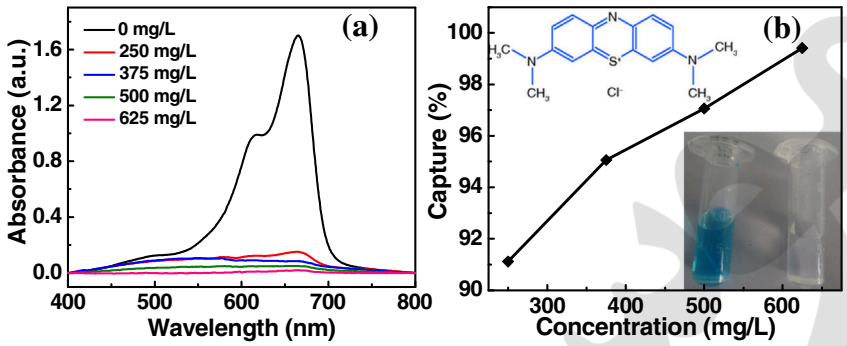

Fig. 4. (a–b) The capture of MB (10 ppm) at different concentrations of QDs-MSN. Lower inset in (b) shows the dye solutions before and after addition of the QDs-MSN (625 mg/L) and upper inset shows the molecular structure of methylene blue (MB).

$$R_L = \frac{1}{1 + K_L C_{Omax}} \quad (4)$$

where, C_{Omax} is the highest initial concentration of dyes used in this study. The value of R_L designates the type of the isotherm to be either linear ($R_L = 1$), favorable ($0 < R_L < 1$), unfavorable ($R_L > 1$), and irreversible ($R_L = 0$) [2].

The second important model to describe adsorption process, is the Freundlich model, and linear form of this model is given by [25]

$$\log Q_e = \log K_F + \frac{1}{n}\log C_e \quad (5)$$

where K_F [(mg/g)(1/mg)$^{1/n}$] indicates adsorption capacity of the QDs-MSN and n indicates how favorable the adsorption process is.

Fig. 5(a) and (b) shows the Langmuir and Freundlich isotherms for the adsorptions of MB onto QDs-MSN. Different adsorption parameters calculated using these two models are compared in Table 2. The acceptability of isotherms is compared by refereeing the correlation coefficient (R^2) for these two models. From the correlation coefficients, it is clearly evident that the Langmuir model describes dye adsorption on composite better than the Freundlich model. In other words, this indicates that the QDs-MSN surface is homogeneous in nature, which would mean that the dye molecules form a monolayer coverage on QDs-MSN surface. The R_L values between 0 and 1 indicate favorable adsorption. In the present study, value of R_L is 0.019, which indicates that this adsorption process of MB on composite surface is a favorable one [26]. In addition, based on the fitted data, the maximum adsorption capacity (Q_m) of MB for this composite is 73.15 mg/g, which shows great capabilities of QDs-MSN's application in cationic dye removal. The n value of higher than 2 indicates good adsorption process [27]. In view of all these, one can easily conclude that the QDs-MSN is an excellent adsorbent material for cationic dye MB.

Table 2
Correlation coefficients and isotherm rate constants for Langmuir and Freundlich models.

Model	Parameters	Values
Langmuir	Q_m (mg/g)	73.15
	K_L (L/mg)	2.16
	R_L	0.019
	R^2	0.999
Freundlich	K_F [(mg/g)(1/mg)$^{1/n}$]	37.93
	n	3.75
	R^2	0.787

3.2.3. Effect of contact time and adsorption kinetics of MB onto QDs-MSN

The adsorption kinetics is determined by observing the behavior of adsorption rate of dye molecules by QDs-MSN over a period. Fig. 6(a) depicts time profiles of MB adsorption on composite for different initial dye concentration over 1 h. As an experimental control, time profile of individual constituent materials (Fig. 6(b)) are also monitored. The dye adsorption capacity and equilibrium contact time are two very important parameters for adsorption studies in terms of practical and economic viability point of view. Generally, dye adsorption capacity of adsorbent increases with the increase in initial dye concentrations. This can be explained by the fact that more no of MB molecules are available for adsorption at higher initial dye concentrations, and it provides higher driving force to overcome the mass transfer resistance of the dye between the aqueous and the solid phase. Therefore, it leads to more no of collisions between dye molecules and active adsorbent sites. A fast adsorption rate is observed in our case for initial concentration ranging from 10 to 50 ppm. A 100% adsorption of MB on QDs-MSN is achieved within 5 min for 10 ppm initial dye

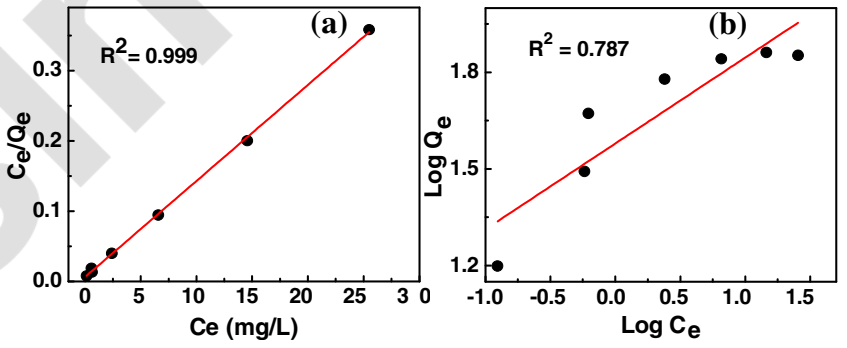

Fig. 5. (a) Langmuir isotherm and (b) Freundlich isotherm of MB onto QDs-MSN (initial concentrations 10–50 ppm).

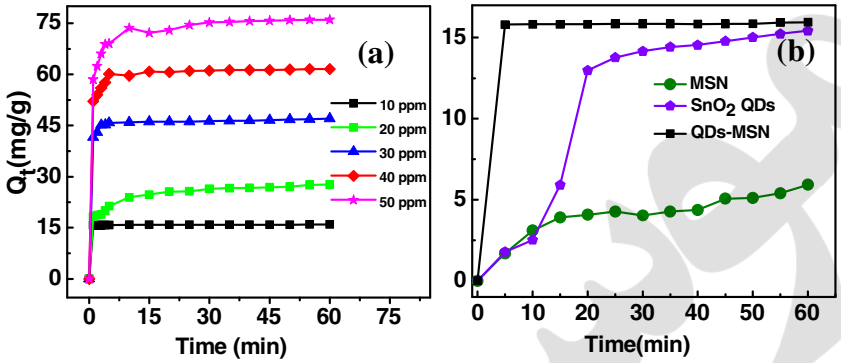

Fig. 6. (a) Time profile of MB adsorption on QDs-MSN composite for different initial dye concentration (10–50 ppm) and (b) time profile of the composite and its constituent materials for 10 ppm dye concentration.

concentration, which is much faster than most of the carbon-based adsorbents [28,29]. Reaching the adsorption equilibrium at a faster rate may be attributed to the increased surface area and reduced diffusion path. Moreover, as compared to other materials, in nanomaterials most of the active sites are happened to be on the exterior surface and easily accessible to adsorbate molecules; leading to a faster equilibrium time [30].

Compared with its counterparts MSN (Fig. 6(b)) as well as SnO_2 QDs, the nanocomposite shows higher adsorption capacity and rate. Li et al. [31] reported that graphene oxide (GO) exhibits higher monolayer adsorption capacity as compared to carbon nanotube (CNT), while CNTs have much larger surface area than GO. This kind of trend cannot be explained by considering the surface area alone. It suggests that the diffusion resistance also plays a major role in determining the adsorption capability and rate of the adsorbents. In spite of comparable Zeta potential and higher surface area MSN offers a lower adsorption capacity as compared to SnO_2 QDs. This essentially establishes that diffusion resistant has a major role to play to decide the adsorption process. The reason for the difference in adsorption rate between pure SnO_2 QDs and nanocomposite may be due to higher negative zeta potential and larger surface area of the composite (see Table 1).

To comprehend the adsorption mechanism and kinetics of adsorption process of MB on QDs-MSN, both pseudo-first-order and pseudo-second-order kinetic models were exploited. These kinetic models can be described by Eqs. (6) and (7) respectively [27]

$$\log(Q_e - Q_t) = \log Q_e - \frac{K_1}{2.303}t \tag{6}$$

$$\frac{t}{Q_t} = \frac{1}{K_2 Q_e^2} + \frac{t}{Q_e} \tag{7}$$

where Q_e and Q_t indicates amounts of dye adsorbed at equilibrium and at time t, respectively. K_1 and K_2 are the rate constants of pseudo-first-order and pseudo-second-order models, respectively. The plots of log $(Q_e - Q_t)$ and t/Q_t vs t for our study are depicted in Fig. 7(a) and (b). The initial adsorption rate (V_O) can also be calculated from the t/Q_t vs t plot, using Eq. (8).

$$V_O = K_2 Q_e^2 K_1 Q_e^2 \tag{8}$$

In many cases pseudo-first-order kinetics is not followed for the complete range of contact time. It may be appropriate for the initial stage of the adsorption processes. Table 3 displays the correlation coefficient and different kinetic model parameters.

The correlation coefficients (R^2) for pseudo-first-order model are comparatively low, and the calculated Q_e values ($Q_{e,cal}$) from this model are not in a good agreement with the experimental data ($Q_{e,exp}$), and hence rules out any possibility that MB adsorption on composite may follow a pseudo-first-order kinetics. On the contrary, for pseudo-second-order model, the theoretical $Q_{e,cal}$ values agree well with experimental data obtained. It also shows a good linearity with R^2 value of 0.999. In view of all these, it can be concluded that, adsorption of MB on QDs-MSN follows a pseudo-second-order model. Table 4 lists the comparison of Q_{max} and equilibrium time for MB on different adsorbents. Comparison of the data collected from literature, establishes the fact that the QDs-MSN with a very short equilibrium time for MB, also has an excellent adsorption capacity as compared to other adsorbent materials.

3.2.4. Effect of solution pH and zeta potentials on dye adsorption

The adsorption of MB on QDs-MSN is a surface phenomenon. Therefore, the pH of the initial solution may affect the active surface binding sites on adsorbent surface, and may affect the aqueous chemistry of the system. Fig. 8(a) describes the effect of pH on the

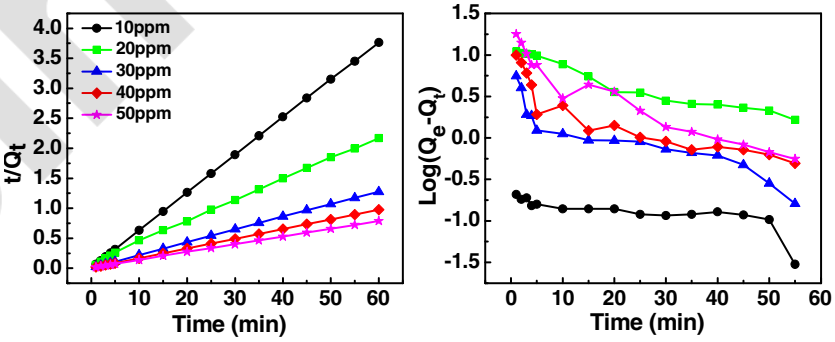

Fig. 7. (a) Pseudo-first-order kinetics and (b) pseudo-second-order kinetics of MB adsorption on QDs-MSN.

Table 3
Summary of the kinetic constants obtained from linear regression of the two models.

C_O (mg/L)	Pseudo first-order kinetics				Pseudo second-order kinetics			
	K_1 (min^{-1})	$Q_{e,cal}$ (mg/g)	$Q_{e,exp}$ (mg/g)	R^2	$K_2 \times 10^{-3}$ (g mg^{-1} min^{-1})	$Q_{e,cal}$ (mg/g)	V_O (mg g^{-1} min^{-1})	R^2
10	0.019	0.19	15.80	0.403	0.507	15.93	128.53	0.999
20	0.032	9.01	31.07	0.898	0.115	28.86	9.62	0.999
30	0.034	1.78	47.00	0.827	0.057	47.08	126.90	0.999
40	0.028	2.30	60.15	0.886	18.13	62.11	212.77	0.999
50	0.05	7.55	69.49	0.930	58.89	77.52	102.04	0.999

Table 4
Summarizes a comparative investigation of previously reported MB adsorbent with the proposed QDs-MSN materials taking into account adsorption capacity and equilibrium time.

Materials	Adsorbent concentration (g/L)	Adsorption capacity (mg/g)	Equilibrium time (min)	Ref.
Ag NPs-AC	–	71.43	15	[32]
Magnetite loaded-MWCNTs	0.40	48.06	120	[28]
Magnetic-MWCNTs	0.50	15.74	360	[29]
RGO based hydrogel	0.60	43.82	120	[33]
MCM-22 zeolite	0.10	55.33	3 days	[34]
QDs-MSN	0.62	73.15	5	Our work

adsorption capacity of MB on QDs-MSN (initial MB concentration:10 ppm; contact time: 5 min). The adsorption capacity of dye steadily increases with the rise in initial solution pH from 3 to 11. pH of the solution may influence the adsorbent's surface charge. At lower pH different groups of dyes and active sites of QDs-MSN, gets protonated and repulsive forces between them decreases the adsorption capacity. In addition, MB can generate cationic pigment (MB^+) in aqueous solution and thus the positive charge on the surface of the adsorbent may inhibit the adsorption of cationic dye in highly acidic solution. [35] With the increase in pH, electrostatic attraction between the negatively charged QDs-MSN composite and cationic MB molecule increases, causing in an increase in the uptake of the dye. At pH 11, there is a decrease in zeta potential and the adsorption capacity. Possibly, at higher basic pH, the material is not stable. The change in the surface charge with pH follows the same behavior as that of the adsorption capacity, which confirms the assumption that the electrostatic forces play a major role in MB adsorption. Similar trends on the effect of adsorption of MB and methyl orange were also reported by Mittal et al. [30], Hameed et al. [36] and Shen et al. [37] respectively.

3.2.5. The effect of temperature on MB adsorption

The effect of temperature on adsorption capacity of MB on QDs-MSN were investigated by varying the temperature while keeping other parameters fixed. Thermodynamic adsorption parameters such as Gibbs energy (ΔG), enthalpy (ΔH) and entropy (ΔS) were calculated from Van't Hoff equation (Eq. (9)) [26,27]

$$\ln\frac{Q_e}{C_e} = \frac{\Delta S}{R} - \frac{\Delta H}{RT} \tag{9}$$

$$\Delta G = \Delta H - T\Delta S \tag{10}$$

where R is the universal gas constant (8.314 J/mol K) and T is absolute temperature. ΔH and ΔS were calculated from the slopes and intercepts of the plot of $\ln\frac{Q_e}{C_e}$ vs $1/T$. The negative value of ΔH establishes that the adsorption process is exothermic in nature. It is confirmed from the negative value of ΔS that MB gets orderly adsorbed on QDs-MSN. The negative value of ΔG demonstrates the spontaneous nature of the adsorption whereas increase in the ΔG value

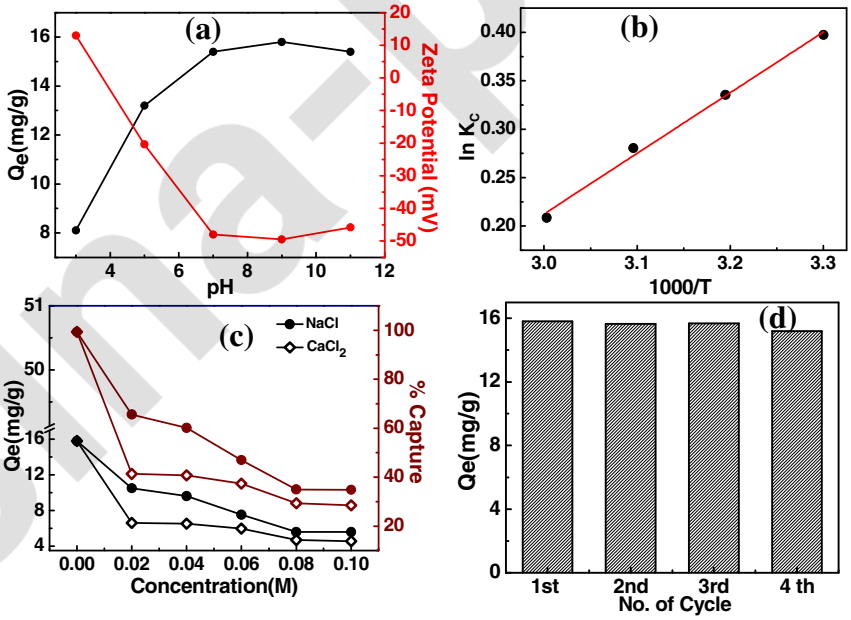

Fig. 8. Effect of (a) solution pH (b) temperature (c) salt concentration on equilibrium adsorption capacity of MB (d) recycling test of QDs-MSN nanocomposite for the adsorption of MB dye (initial dye concentration: 10 ppm [except 50 ppm for temperature dependent study]; contact time: 5 min).

Table 5
Thermodynamic parameters for MB adsorption on QDs-MSN.

ΔH (kJ/mol)	ΔS (J/mol K)	ΔG (kJ/mol)			
		303 K	313 K	323 K	333 K
−5.2	−13.84	−1.00	−0.991	−0.964	−0.578

with increased temperature indicates more effective adsorption at lower temperature. The results are presented in Table 5.

3.2.6. Effect of salt concentration on adsorption of MB

The dyes in wastewater of textile industry usually contain higher salt concentration too, and ionic strength may affect the adsorption process. Fig. 8(c) shows the effect of ionic strength (salt concentration) on the adsorption capacity or capture percentage. With the increase in the salt concentration there is a decrease of MB adsorption on QDs-MSN. Cationic dye MB may compete with other cations, for the available active sites of negatively charged QDs-MSN. As the salt concentration increases from 0 to 0.1 M, the adsorption capacity of MB decreases from 15.8 to 5.57 mg/g for NaCl and 4.56 mg/g for $CaCl_2$; while the capture percentage decreases from 99.4% to 34.8% and 28.5%, respectively. In addition, the increase in the salt concentration may shield the charge on MB, which results in the decrease of removal efficiency. Moreover, for the same concentration of NaCl and $CaCl_2$, a lower adsorption efficiency is observed for Ca^{+2} due to its higher ionic strength.

3.2.7. Effect of recycling adsorbents on MB adsorption

Due to rigorous ecological and commercial demands for sustainability, repeated reuse of adsorbents is an important parameter for routine applications. In order to significantly reduce the overall cost of adsorption process, an adsorbent should not only have high adsorption capability, but also good desorption properties. From Fig. 8(b) it is evident that, the adsorption efficiency of the nanocomposite is retained even after 4th cycle of reuse. Reusability of the QDs-MSN essentially establishes that this material has enough potential for industrial applications. To overrule the possibility of tin leaching into the supernatant solution, ICP-MS measurements were carried out. It shows that the concentration of tin in the supernatant solution is below 2 ppb; but as reported by World Health Organization the water supplies in the USA contains tin in the range of 1.1–2.2 μg/litre (maximum 30 μg/litre).

4. Conclusion

A simple two-step method has been developed to fabricate the QDs-MSN nanocomposite, in which MSN is uniformly loaded with SnO_2 QDs. This nanocomposite exhibits a higher surface area with a uniform pore size distribution. Using QDs-MSN as adsorbent, 100% capture of MB is achieved within 5 min. Faster achievement of the adsorption equilibrium may be ascribed to the increased surface area and reduced diffusion path. The adsorption behavior is best described by Langmuir isotherm ($R^2 > 0.999$) and it follows a pseudo second order kinetics. This adsorption of MB by the nanocomposite is homogeneous in nature and mainly controlled by electrostatic interaction between negative polarity adsorbent and cationic adsorbate. The nanocomposite exhibits exciting maximum adsorption capacity (Q_m = 73.15 mg/g) toward MB. The recycling experiment shows that the materials can easily be regenerated after washing with MilliQ water and the regenerated materials showed no significant loss in adsorption capacity even up to the fourth cycle. The high adsorption capacity, fast removal rate and reusability of the QDs-MSN nanocomposite essentially establishes that this material has the potential to be used as environment friendly and low cost adsorbent material for industrial applications.

Author contributions

All the authors have contributed equally for this work and given approval to the final version of the manuscript.

Acknowledgements

The financial support by nanomission of DST, Govt. of India is gratefully acknowledged. Dipa Dutta acknowledges CSIR, India for the award of Senior Research Fellowship (SRF). We acknowledge the central characterization facilities at IIT Bombay.

Appendix A. Supplementary data

Supplementary data associated with this article can be found, in the online version, at http://dx.doi.org/10.1016/j.cej.2015.06.110.

References

[1] T. Liu, Y. Li, Q. Du, J. Sun, Y. Jiao, G. Yang, Z. Wang, Y. Xia, W. Zhang, K. Wang, H. Zhu, D. Wu, Adsorption of methylene blue from aqueous solution by graphene, Colloids Surf. B 90 (2012) 197–203.
[2] E.N. El Qada, S.J. Allen, G.M. Walker, Adsorption of methylene blue onto activated carbon produced from steam activated bituminous coal: a study of equilibrium adsorption isotherm, Chem. Eng. J. 124 (2006) 103–110.
[3] S. Ray, M. Takafuji, H. Ihara, Peptide-based surface modified silica particles: adsorption materials for dye-loaded wastewater treatment, RSC Adv. 3 (2013) 23664–23672.
[4] B.H. Hameed, A.T. Din, A.L. Ahmad, Adsorption of methylene blue onto bamboo-based activated carbon: kinetics and equilibrium studies, J. Hazard. Mater. 141 (2007) 819–825.
[5] S. Eftekhari, A. Habibi-Yangjeh, S. Sohrabnezhad, Application of AlMCM-41 for competitive adsorption of methylene blue and rhodamine B: thermodynamic and kinetic studies, J. Hazard. Mater. 178 (2010) 349–355.
[6] S. Singh, K.C. Barick, D. Bahadur, Fe_3O_4 embedded ZnO nanocomposites for the removal of toxic metal ions, organic dyes and bacterial pathogens, J. Mater. Chem. A 1 (2013) 3325–3333.
[7] A.H. Karim, A.A. Jalil, S. Triwahyono, S.M. Sidik, N.H. Kamarudin, R. Jusoh, N.W. Jusoh, B.H. Hameed, Amino modified mesostructured silica nanoparticles for efficient adsorption of methylene blue, J. Colloid Interface Sci. 386 (2012) 307–314.
[8] T. Madrakiana, A. Afkhami, M. Ahmadi, H. Bagheri, Removal of some cationic dyes from aqueous solutions using magnetic-modified multi-walled carbon nanotubes, J. Hazard. Mater. 196 (2011) 109–114.
[9] S.-Y. Mak, D.-H. Chen, Fast adsorption of methylene blue on polyacrylic acid-bound iron oxide magnetic nanoparticles, Dyes Pigm. 61 (2004) 93–98.
[10] X. Zhang, P. Zhang, Z. Wu, L. Zhang, G. Zeng, C. Zhou, Adsorption of methylene blue onto humic acid-coated Fe_3O_4 nanoparticles, Colloids Surf. A 435 (2013) 85–90.
[11] Y. Wang, X. Zhang, X. He, W. Zhang, C. Lu, In situ synthesis of MnO_2 coated cellulose nanofibers hybrid for effective removal of methylene blue, Carbohydr. Polym. 110 (2014) 302–308.
[12] W.J. Tseng, R.D. Lin, $BiFeO_3$/alpha-Fe_2O_3 core/shell composite particles for fast and selective removal of methyl orange dye in water, J. Colloid Interface Sci. 428 (2014) 95–100.
[13] M.N. Ahmed, R.N. Rm, Removal of basic dye from waste-water using silica as adsorbent, Environ. Pollut. 77 (1992) 79–86.
[14] K.-E. You, J.-H. Park, Y.C. Kim, S.-G. Oh, Magnetic properties and dye adsorption capacities of silica–hematite nanocomposites with well-defined structures prepared in surfactant solutions, Solid State Sci. 33 (2014) 38–44.
[15] A. Shamsizadeh, M. Ghaedi, A. Ansari, S. Azizian, M.K. Purkait, Tin oxide nanoparticle loaded on activated carbon as new adsorbent for efficient removal of malachite green-oxalate: non-linear kinetics and isotherm study, J. Mol. Liq. 195 (2014) 212–218.
[16] S. Zhuang, X. Xu, Y. Pang, J. Hu, C. Yang, L. Tong, Y. Zhou, PEGME-bonded SnO_2 quantum dots for excellent photocatalytic activity, RSC Adv. 3 (2013) 20422–20428.
[17] N. Shanta Singh, H. Kulkarni, L. Pradhan, D. Bahadur, A multifunctional biphasic suspension of mesoporous silica encapsulated with YVO4:Eu3+ and Fe_3O_4 nanoparticles: synergistic effect towards cancer therapy and imaging, Nanotechnology 24 (2013) 065101.
[18] F. Lu, S.H. Wu, Y. Hung, C.Y. Mou, Size effect on cell uptake in well-suspended, uniform mesoporous silica nanoparticles, Small 5 (2009) 1408–1413.
[19] L.L. Hench, J.K. West, The sol gel process, Chem. Rev. 90 (1990) 33–72.

[20] Y.D. Wang, C.L. Ma, H.D. Li, S. Zhang, Synthesis and characterization of the composite of SnO_2 nanoparticles coated on SiO_2 microspheres, Mater. Chem. Phys. 107 (2008) 248–253.
[21] D. Dutta, S. Chandra, A.K. Swain, D. Bahadur, SnO_2 quantum dots-reduced graphene oxide composite for enzyme-free ultrasensitive electrochemical detection of urea, Anal. Chem. 86 (2014) 5914–5921.
[22] K.S.W. Sing, Reporting physisorption data for gas/solid systems, Pure Appl. Chem. 54 (1982) 2201–2218.
[23] X. Yuan, Y. Wang, J. Wang, C. Zhou, Q. Tang, X. Rao, Calcined graphene/MgAl-layered double hydroxides for enhanced Cr(VI) removal, Chem. Eng. J. 221 (2013) 204–213.
[24] S. Luo, X. Xu, G. Zhou, C. Liu, Y. Tang, Y. Liu, Amino siloxane oligomer-linked graphene oxide as an efficient adsorbent for removal of Pb(II) from wastewater, J. Hazard. Mater. 274 (2014) 145–155.
[25] M.M. Ayad, A.A. El-Nasr, Adsorption of cationic dye (methylene blue) from water using polyaniline nanotubes base, J. Phys. Chem. C 114 (2010) 14377–14383.
[26] L. Ai, C. Zhang, Z. Chen, Removal of methylene blue from aqueous solution by a solvothermal-synthesized graphene/magnetite composite, J. Hazard. Mater. 192 (2011) 1515–1524.
[27] Y. Yang, Y. Xie, L. Pang, M. Li, X. Song, J. Wen, H. Zhao, Preparation of reduced graphene oxide/poly(acrylamide) nanocomposite and its adsorption of Pb(II) and methylene blue, Langmuir 29 (2013) 10727–10736.
[28] L. Ai, C. Zhang, F. Liao, Y. Wang, M. Li, L. Meng, J. Jiang, Removal of methylene blue from aqueous solution with magnetite loaded multi-wall carbon nanotube: kinetic, isotherm and mechanism analysis, J. Hazard. Mater. 198 (2011) 282–290.
[29] J.L. Gong, B. Wang, G.M. Zeng, C.P. Yang, C.G. Niu, Q.Y. Niu, W.J. Zhou, Y. Liang, Removal of cationic dyes from aqueous solution using magnetic multi-wall carbon nanotube nanocomposite as adsorbent, J. Hazard. Mater. 164 (2009) 1517–1522.
[30] H. Mittal, N. Ballav, S.B. Mishra, Gum ghatti and Fe_3O_4 magnetic nanoparticles based nanocomposites for the effective adsorption of methylene blue from aqueous solution, J. Ind. Eng. Chem. 20 (2014) 2184–2192.
[31] Y. Li, Q. Du, T. Liu, X. Peng, J. Wang, J. Sun, Y. Wang, S. Wu, Z. Wang, Y. Xia, L. Xia, Comparative study of methylene blue dye adsorption onto activated carbon, graphene oxide, and carbon nanotubes, Chem. Eng. Res. Des. 91 (2013) 361–368.
[32] M. Ghaedi, S. Heidarpour, S.N. Kokhdan, R. Sahraie, A. Daneshfar, B. Brazesh, Comparison of silver and palladium nanoparticles loaded on activated carbon for efficient removal of methylene blue: kinetic and isotherm study of removal process, Powder Technol. 228 (2012) 18–25.
[33] J.N. Tiwari, K. Mahesh, N.H. Le, K.C. Kemp, R. Timilsina, R.N. Tiwari, K.S. Kim, Reduced graphene oxide-based hydrogels for the efficient capture of dye pollutants from aqueous solutions, Carbon 56 (2013) 173–182.
[34] H.L. Shaobin Wang, Longya Xu, Application of zeolite MCM-22 for basic dye removal from wastewater, J. Colloid Interface Sci 295 (2006) 71–78.
[35] L. Cui, X. Guo, Q. Wei, Y. Wang, L. Gao, L. Yan, T. Yan, B. Du, Removal of mercury and methylene blue from aqueous solution by xanthate functionalized magnetic graphene oxide: sorption kinetic and uptake mechanism, J. Colloid Interface Sci. 439 (2015) 112–120.
[36] B.H. Hameed, A.A. Ahmad, Batch adsorption of methylene blue from aqueous solution by garlic peel, an agricultural waste biomass, J. Hazard. Mater. 164 (2009) 870–875.
[37] J. Shen, Z. Li, Y.-N. Wu, B. Zhang, F. Li, Dendrimer-based preparation of mesoporous alumina nanofibers by electrospinning and their application in dye adsorption, Chem. Eng. J. 264 (2015) 48–55.